Interacción magnetostática en microhilos ferromagnéticos biestables

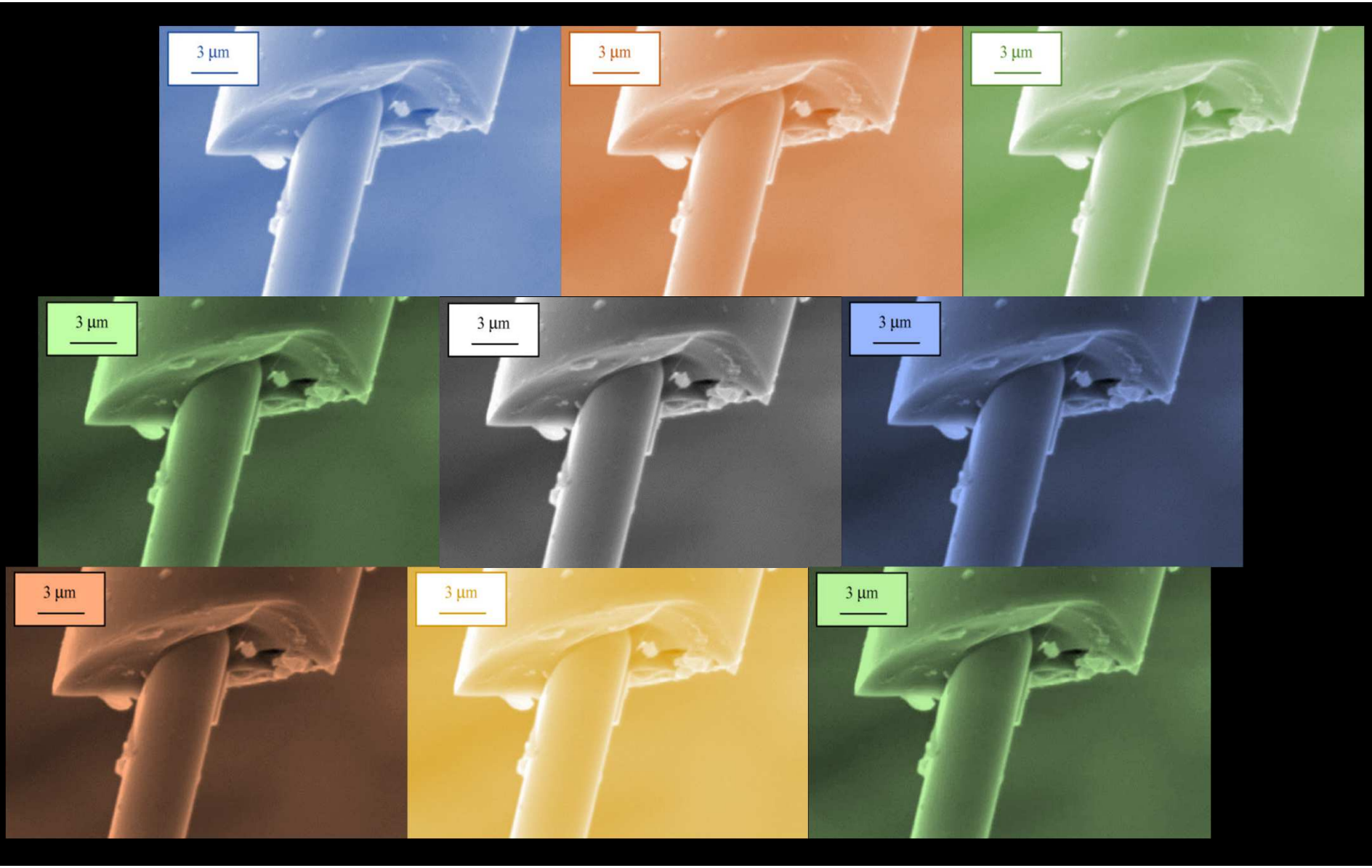
3 µm
3 µm
3 µm
3 µm
3 µm
3 µm
3 µm
3 µm
3 µm

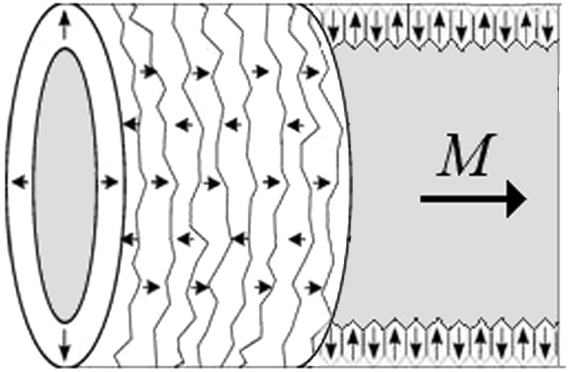

Estructura de dominios de un microhilo
con magnetostricción positiva

PHYSICAL REVIEW B VOLUME 61, NUMBER 13 1 APRIL 2000-I

Magnetic microwires as macrospins in a long-range dipole-dipole interaction

L. C. Sampaio,* E. H. C. P. Sinnecker, and G. R. C. Cernicchiaro
Centro Brasileiro de Pesquisas Físicas/CNPq, Rua Dr. Xavier Sigaud, 150, URCA, 22290-180, Rio de Janeiro, RJ, Brazil

M. Knobel
Instituto de Física ''Gleb Wataghin,'' Universidade Estadual de Campinas (UNICAMP), Caixa Postal 6165, Campinas 13083-970, SP, Brazil

M. Vázquez and J. Velázquez†
Instituto de Magnetismo Aplicado (UCM/RENFE) and Instituto de Ciencia de Materiales (CSIC), PO Box 155, 28230 Las Rozas, Madrid, Spain
(Received 15 October 1999)

glass-coated amorphous $Fe_{77.5}Si_{7.5}B_{15}$ microwire with diameter of 5 μm and lengths from 5 to 60 mm

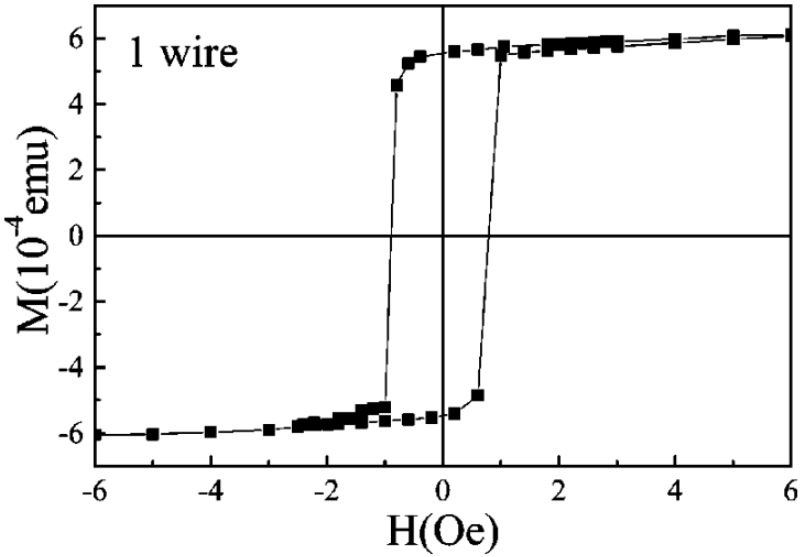

FIG. 1. Hysteresis loop for one microwire at room temperature. The reversal field is -0.89 Oe for negative reversal field and 0.79 Oe for positive reversal field. The coercive field is defined as the mean value, $|H_C| = 0.85$ Oe.

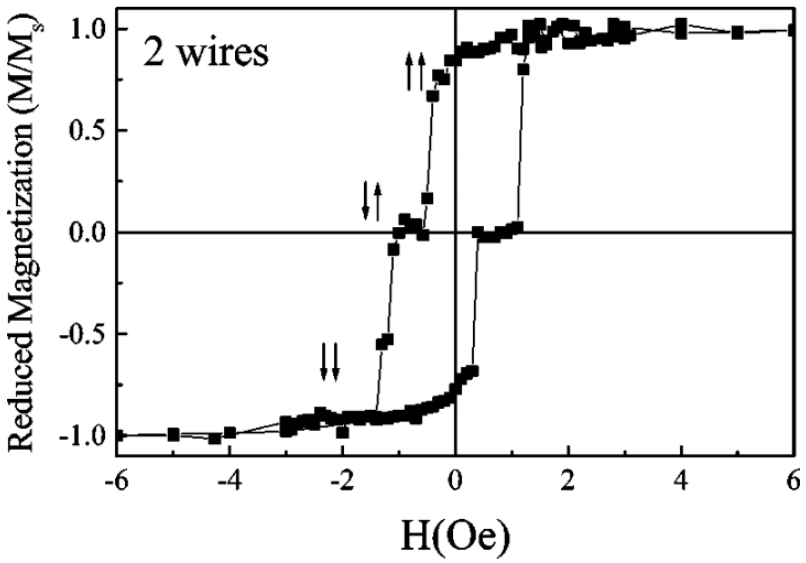

FIG. 2. Hysteresis loop for two microwires at room temperature. The mean reversal fields on the demagnetization are $H_2^i = -0.43$ Oe and $H_2^{ii} = -1.11$ Oe. The magnetization is normalized to the saturation value. The arrows represent the magnetic configuration of the wires.

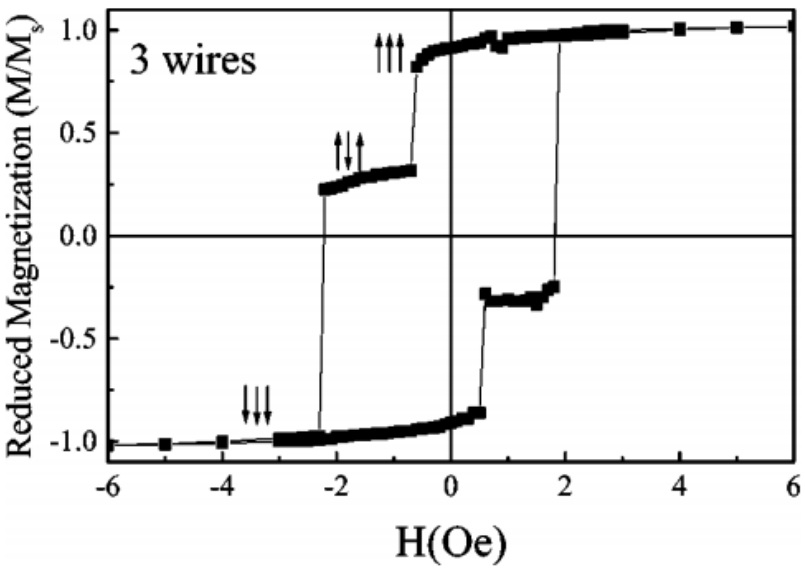
3 wires
Reduced Magnetization (M/M$_s$)
1.0
0.5
0.0
-0.5
-1.0
-6
-4
-2
0
2
4
6
H(Oe)

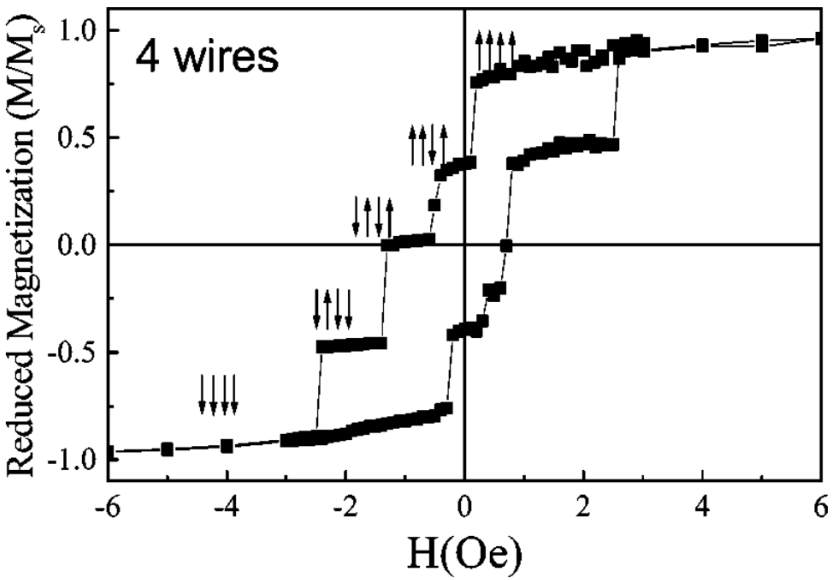
4 wires
Reduced Magnetization (M/M$_s$)
1.0
0.5
0.0
-0.5
-1.0
-6
-4
-2
0
2
4
6
H(Oe)

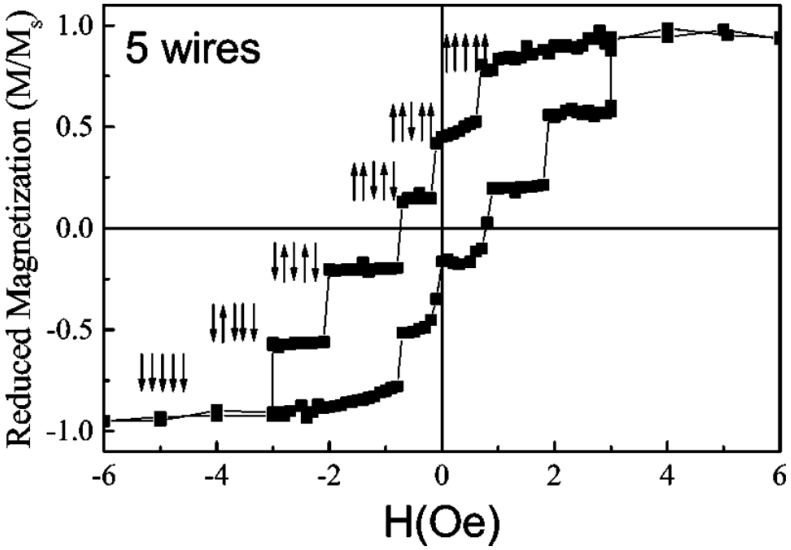
5 wires
Reduced Magnetization (M/M$_s$)
1.0
0.5
0.0
-0.5
-1.0
-6
-4
-2
0
2
4
6
H(Oe)

$H_{i,j}$ is the field of the wire i over the wire j

$$\mathbf{H}_{i,j} = -K_n \mathbf{M}_i$$

where K_n is a geometric factor and $\mathbf{M}_i$ is the magnetization

n denotes the distance between the wires

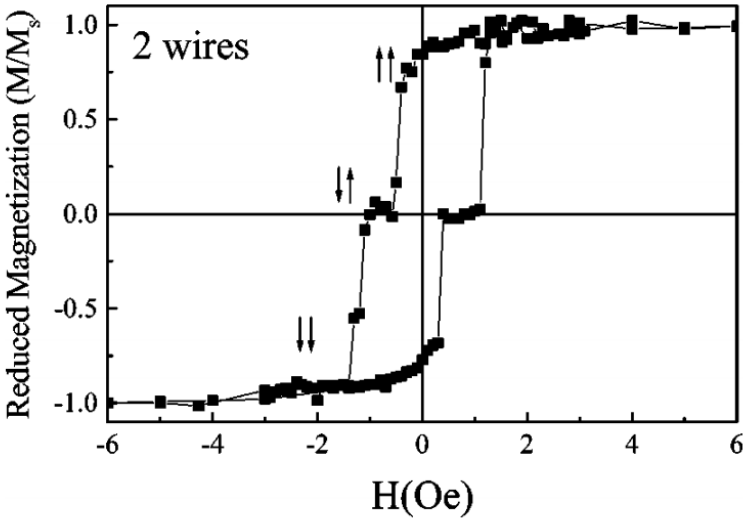

$$H_2^i = H_C - K_1 M$$

$$H_2^{ii} = H_C + K_1 M$$

2 wires			
$\uparrow\uparrow$	$\downarrow\uparrow$	$H_2^i = H_C - K_1 M$	-0.43
$\downarrow\uparrow$	$\downarrow\downarrow$	$H_2^i = H_C + K_1 M$	-1.11
3 wires			
$\uparrow\uparrow\uparrow$	$\uparrow\downarrow\uparrow$	$H_3^i = H_C - 2K_1 M$	-0.63
$\uparrow\downarrow\uparrow$	$\downarrow\downarrow\uparrow$	$H_3^{ii} = H_C - (K_1 - K_2) M$	*
$\downarrow\downarrow\uparrow$	$\downarrow\downarrow\downarrow$	$H_3^{iii} = H_C + (K_1 + K_2) M$	*
4 wires			
$\uparrow\uparrow\uparrow\uparrow$	$\uparrow\uparrow\downarrow\uparrow$	$H_4^i = H_C - (2K_1 + K_2) M$	0.16
$\uparrow\uparrow\downarrow\uparrow$	$\downarrow\uparrow\downarrow\uparrow$	$H_4^{ii} = H_C - (K_1 - K_2 + K_3) M$	-0.45
$\downarrow\uparrow\downarrow\uparrow$	$\downarrow\uparrow\downarrow\downarrow$	$H_4^{iii} = H_C + (K_1 - K_2 + K_3) M$	-1.35
$\downarrow\uparrow\downarrow\downarrow$	$\downarrow\downarrow\downarrow\downarrow$	$H_4^{iv} = H_C + (2K_1 + K_2) M$	-2.45
5 wires			
$\uparrow\uparrow\uparrow\uparrow\uparrow$	$\uparrow\uparrow\downarrow\uparrow\uparrow$	$H_5^i = H_C - (2K_1 + 2K_2) M$	0.69
$\uparrow\uparrow\downarrow\uparrow\uparrow$	$\downarrow\uparrow\downarrow\uparrow\uparrow$	$H_5^{ii} = H_C - (K_1 - K_2 + K_3 + K_4) M$	-0.13
$\downarrow\uparrow\downarrow\uparrow\uparrow$	$\downarrow\uparrow\downarrow\uparrow\downarrow$	$H_5^{iii} = H_C - (K_1 - K_2 + K_3 - K_4) M$	-0.73
$\downarrow\uparrow\downarrow\uparrow\downarrow$	$\downarrow\uparrow\downarrow\downarrow\downarrow$	$H_5^{iv} = H_C + (2K_1 - K_2 + K_3) M$	-1.90
$\downarrow\uparrow\downarrow\downarrow\downarrow$	$\downarrow\downarrow\downarrow\downarrow\downarrow$	$H_5^{v} = H_C + (2K_1 + K_2 + K_3) M$	-3.0

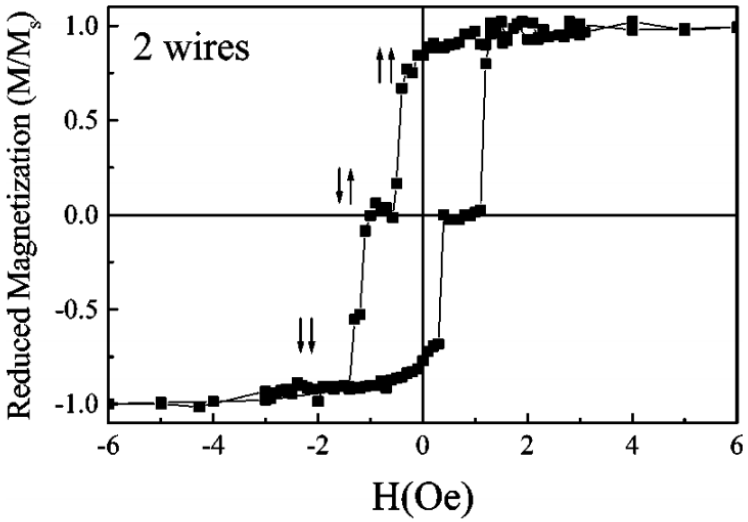

Monte Carlo

fore, we have used the Monte Carlo (MC) method based on a one-dimensional modified classical Ising model. We have considered a one-dimensional array of magnetic moments interacting through the long-range dipole-dipole interaction. In our model, the Hamiltonian takes a simple form,

$$H = M^2 \sum J_{ij}\sigma_i\sigma_j - (H + H_{ani}) \sum \sigma_i , \qquad (9)$$

where the variable σ_i takes the values ± 1 on a site i on a one-dimensional array, allowing the magnetic moments to point up ($\sigma_i = +1$) or down ($\sigma_i = -1$) along an axis perpendicular to the axis of the array. The first summation in Eq. (9) denotes the dipole-dipole interaction acting over all pairs of magnetic moments. The constant of coupling J_{ij} is identified with $1/K_n$ [see Eq. (5)], and the distances between the magnetic moments, r_{ij}, are measured in units of the lattice constant a. Note that the magnetization, **M**, of a wire is given

Monte Carlo

We used the single-spin-flip Metropolis dynamics and open boundary conditions (details of calculations are given in a previous publication).[4] The hysteresis loops were calculated changing the field H with a sweep rate of 10 MC steps for each magnetization value. The temperature (T) was considered low enough in order to be well below the antiferromagnetic-paramagnetic phase transition. The values

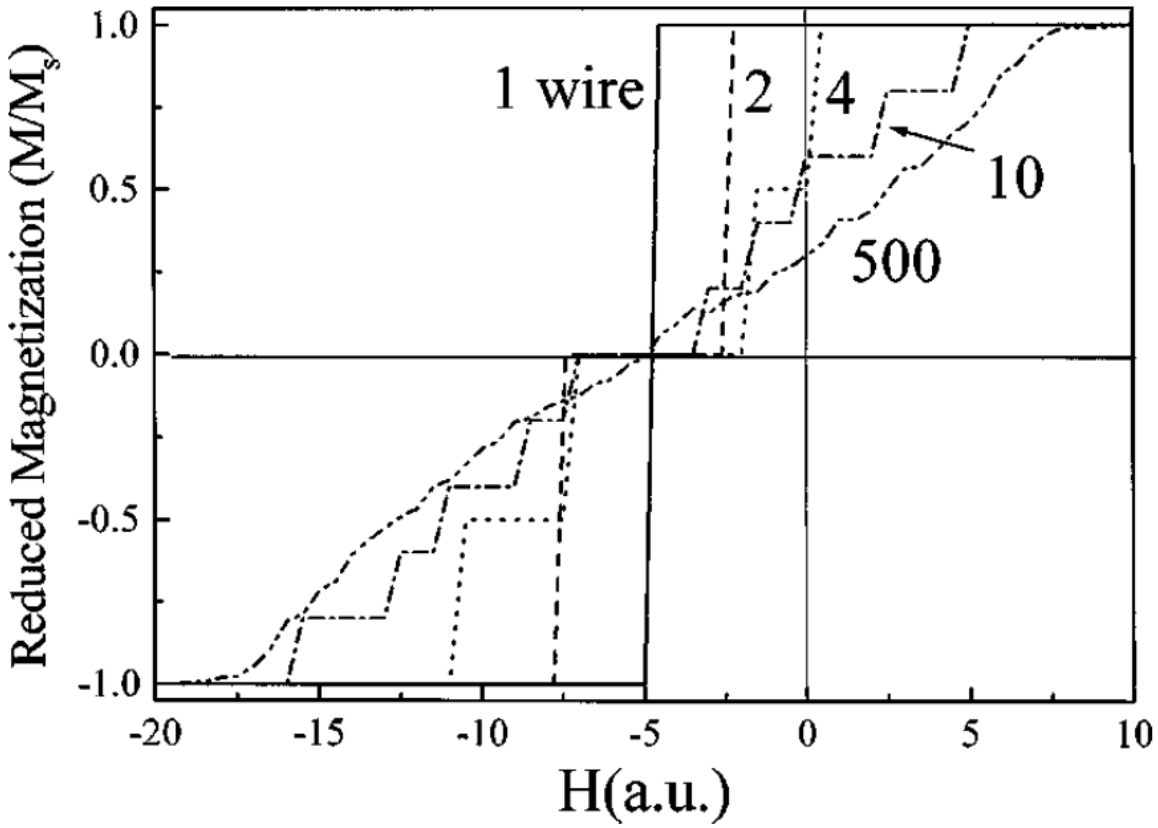

FIG. 7. Demagnetization region of hysteresis loop calculated using the Monte Carlo method for 1 wire and for arrays of 2, 4, 10, and 500 wires.

Interacción magnetostática en microhilos ferromagnéticos biestables

Mendoza Zélis P.[1*], Pasquevich G. A.[1], Sánchez F. H.[1], Vazquez M.[2], B. Pianciola[1]

Departamento de Física, Facultad de Ciencias Exactas, Universidad Nacional de La Plata - IFLP-CONICET; La Plata , Argentina.

Instituto de Ciencia de Materiales de Madrid, 28049 Cantoblanco, CSIC, España

Muestras estudiadas:

Dimensiones:

Diámetro núcleo metálico: 13 μm

Diámetro total: 20 μm

argo: 30mm

Composición:

$Fe_{58.9}\ Co_{14.7}\ Si_{16.2}\ B_{10.2}$

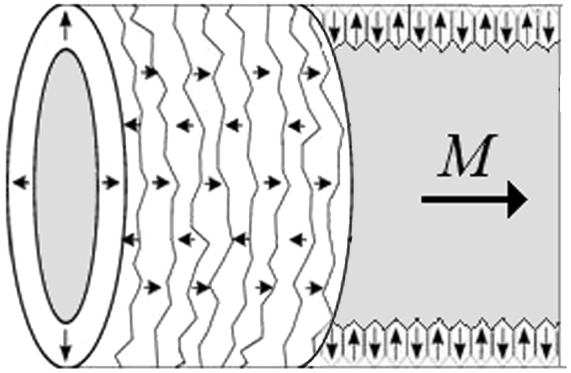

Estructura de dominios de un microhilo con magnetostricción positiva

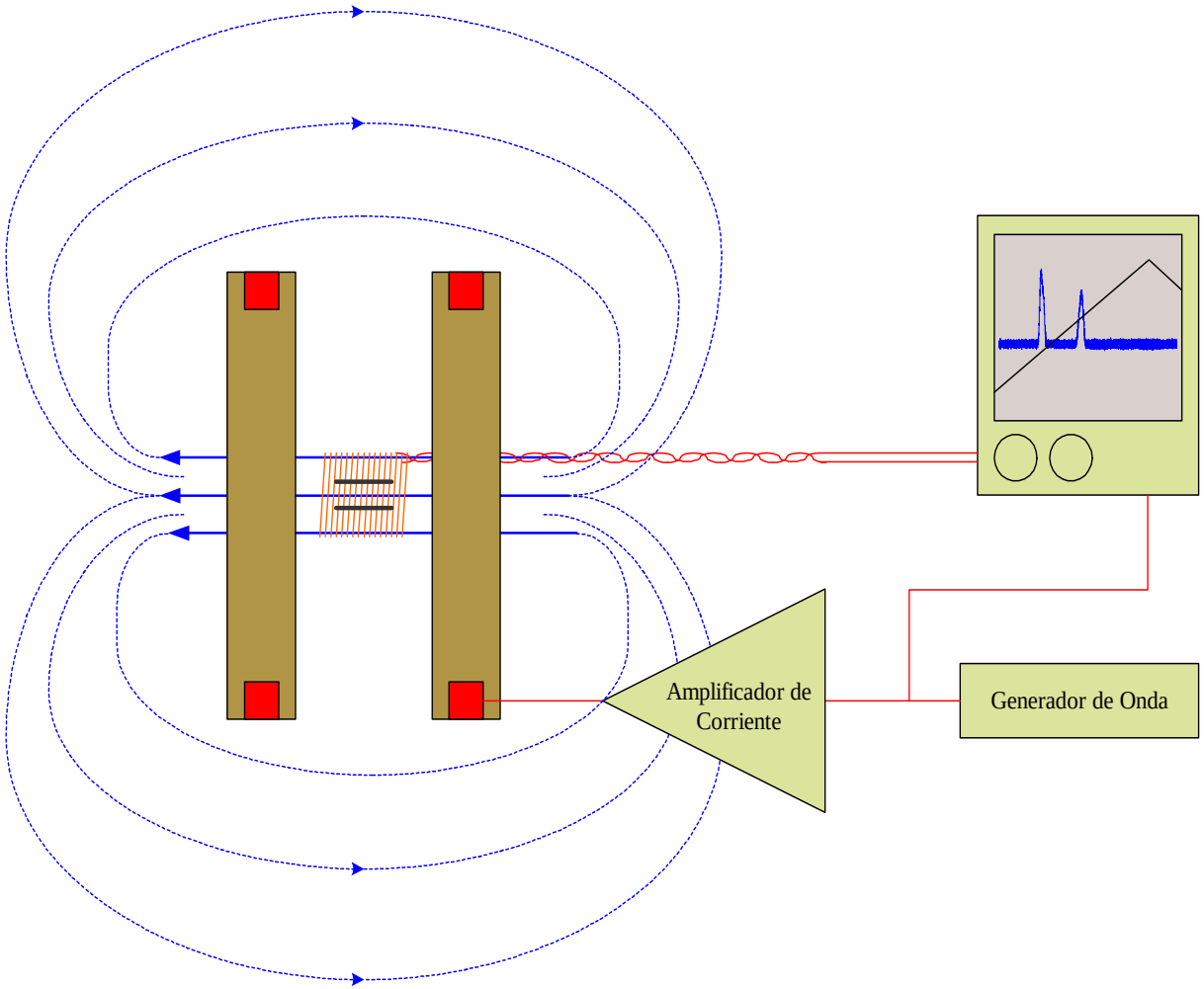

Osciloscopio
Tektronix TDS3012
100 MHz

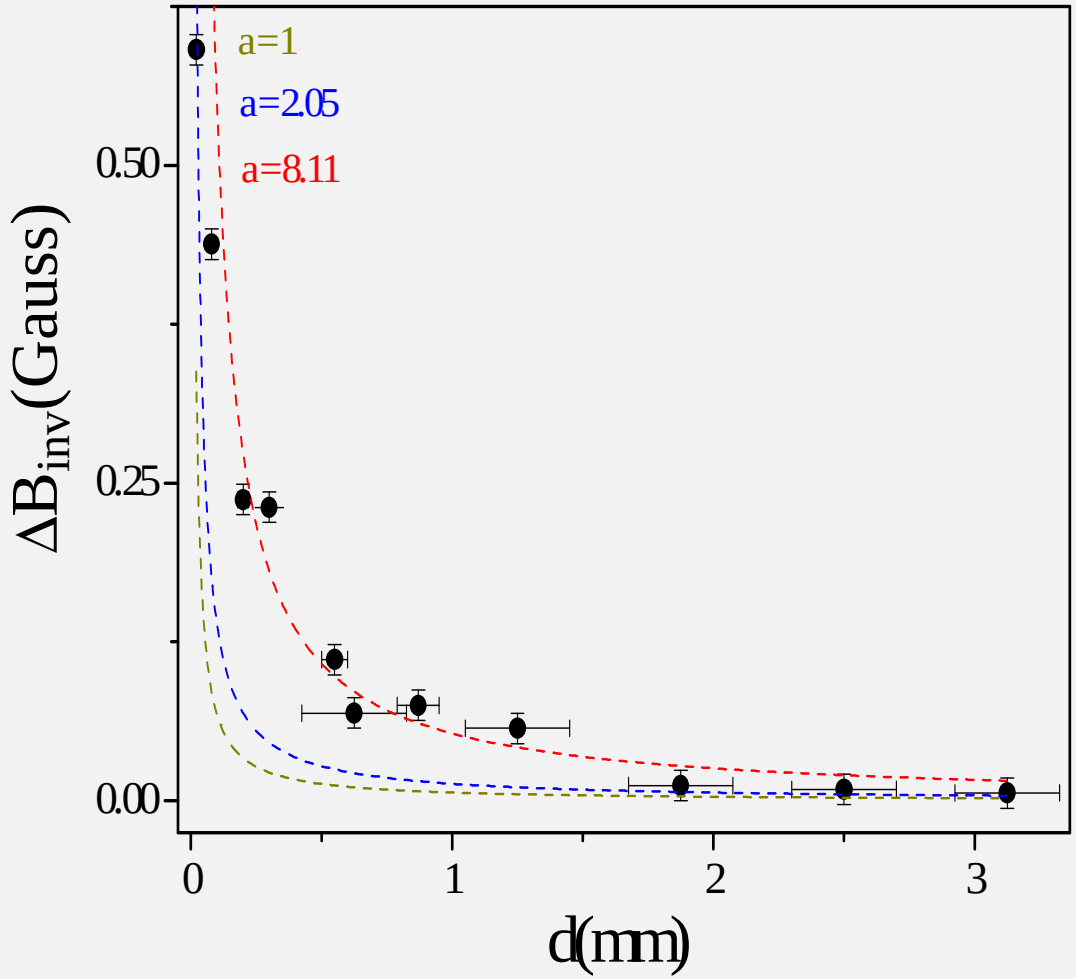

$$B_{cr} = a\frac{\mu_0}{8l} M_S D^2 \left(\frac{1}{d} - \frac{1}{\left(d^2 + l^2\right)^{1/2}} \right)$$

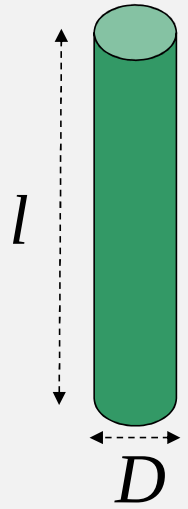

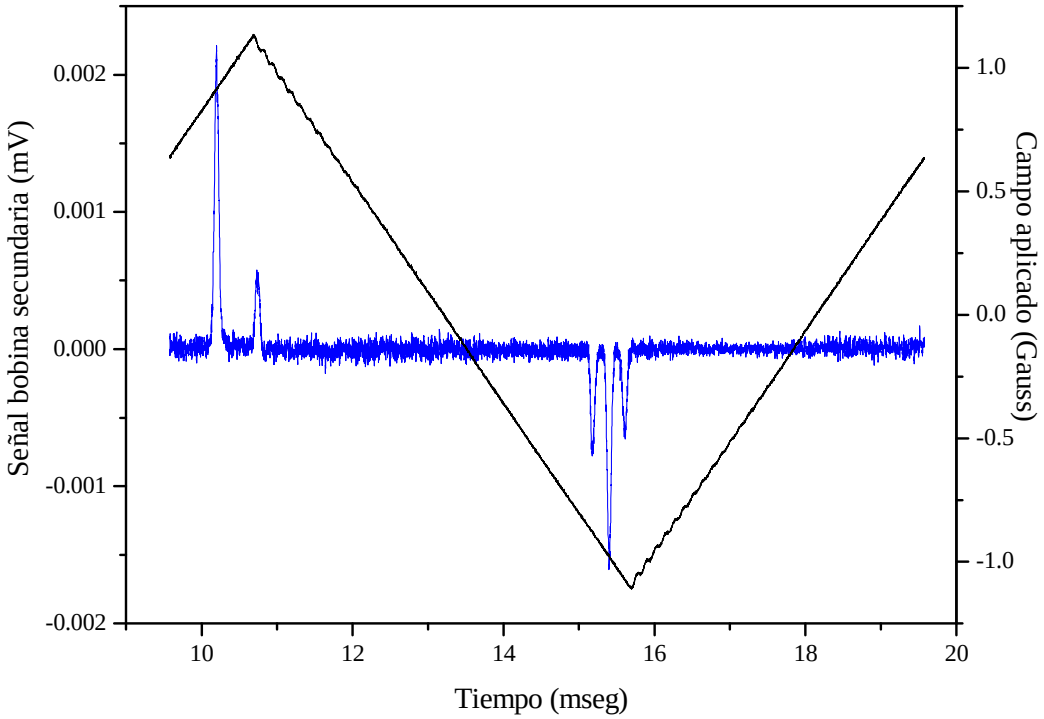

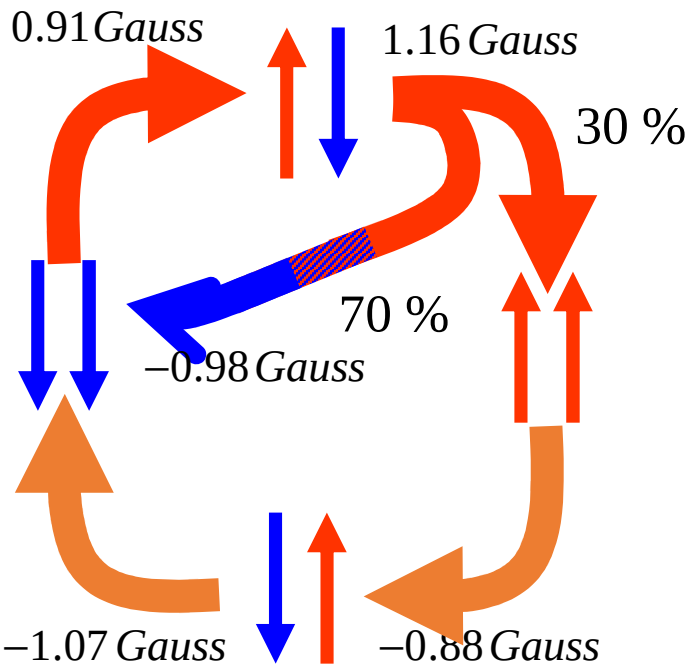

Medidas registradas con un campo máximo aplicado de 1.16 Gauss y una frecuencia de 100 Hz (izquierda). Esquema de los procesos de inversión de la magnetización de los microhilos. (derecha).

PHYSICAL REVIEW B **96**, 174427 (2017)

Effective demagnetizing tensors in arrays of magnetic nanopillars

P. Mendoza Zélis,[1,2] V. Vega,[3] V. M. Prida,[3] L. C. Costa-Arzuza,[4] F. Béron,[5]
K. R. Pirota,[5] R. López-Ruiz,[5,*] and F. H. Sánchez[1,†]

Diámetro D = 52 ± 2 nm
Longitud L = 100 ± 6 nm
Relación de aspecto λ=1.9±0.1

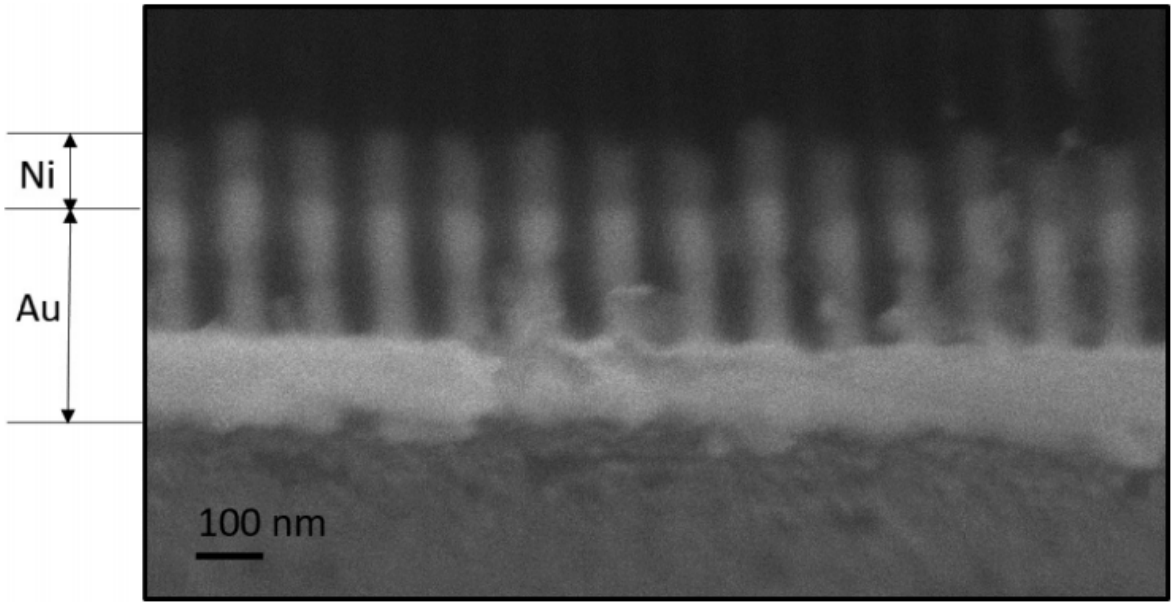

FIG. 1. Cross-sectional view of nickel NP array.

specimen	Diameter (nm)	electrodepo-sition time (s)	Wire Length (just Ni)
L1	35	5	130
L2	35	20	460
L3	35	10	150
L4	52	10	155
L5	52	5	100
L6	52	20	350

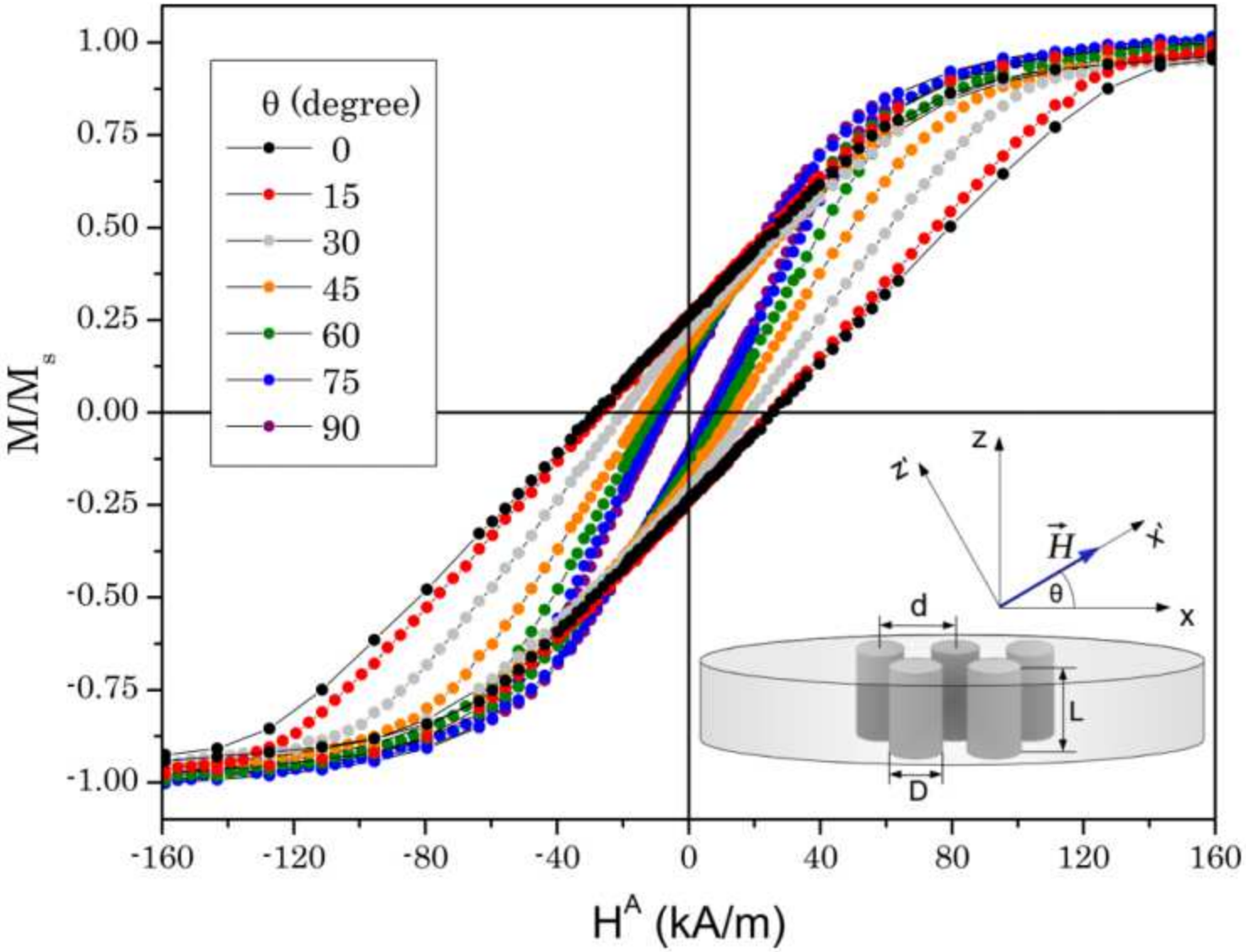
θ (degree)
0
15
30
45
60
75
90
M/M_s
1.00
0.75
0.50
0.25
0.00
-0.25
-0.50
-0.75
-1.00
-160
-120
-80
-40
0
40
80
120
160
H^A (kA/m)
z
z'
x
x'
H
θ
d
L
D

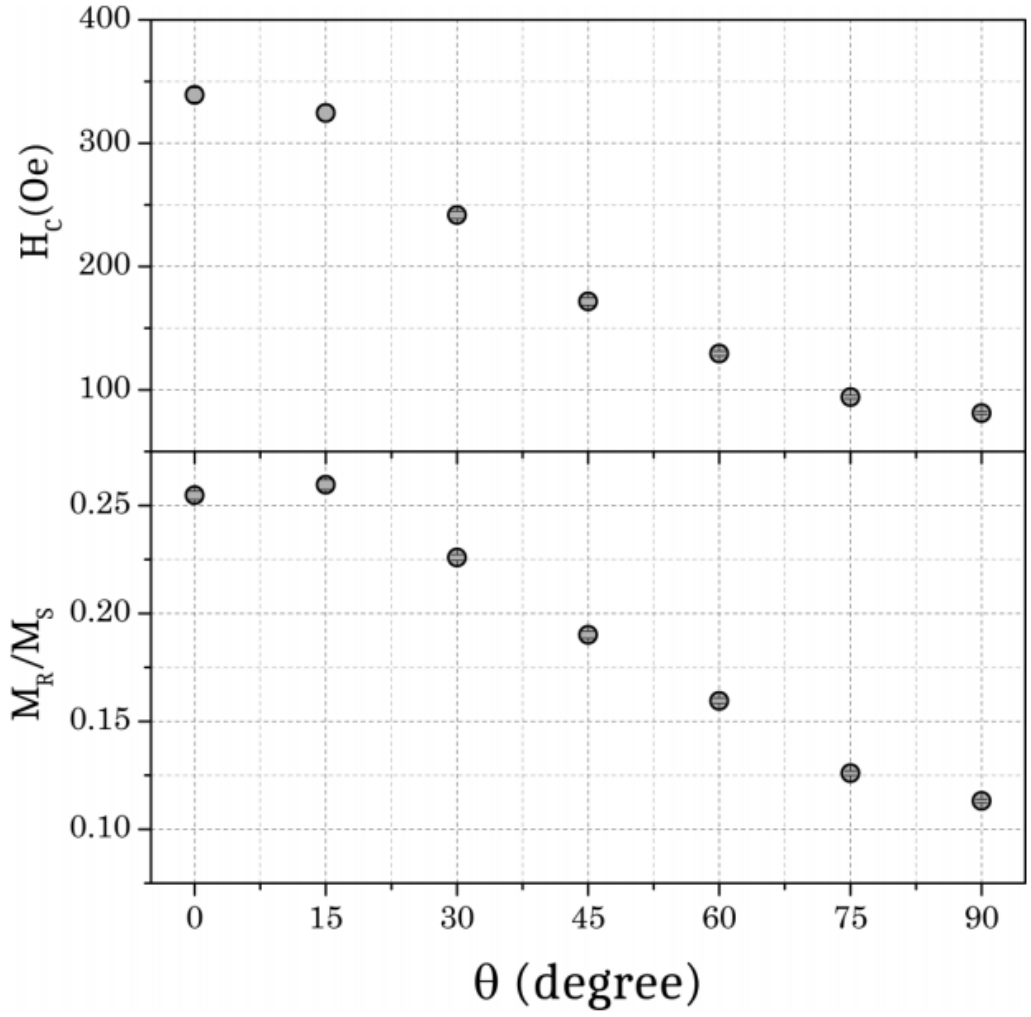
400
300
200
100
H_c(Oe)
0.25
0.20
0.15
0.10
M_R/M_S
0
15
30
45
60
75
90
θ (degree)

JOURNAL OF APPLIED PHYSICS VOLUME 37, NUMBER 13 DECEMBER 1966

Ballistic Demagnetizing Factor in Uniformly Magnetized Cylinders

R. I. JOSEPH*
Raytheon Research Division, Waltham, Massachusetts
(Received 31 May 1966)

The magnetometric demagnetizing factor N_m, defined as the volume average of the spatially varying demagnetizing factor, may be written for the present case as

$$N_m = 1 - (4/3\pi p)\{(1+p^2)^{\frac{1}{2}} \times [p^2 K(\kappa) + (1-p^2)E(\kappa)] - 1\}, \quad (11)$$

where

$$\kappa^2 = (1+p^2)^{-1}, \quad (12)$$

$K(k)$ and $E(k)$ are the complete elliptic integrals of the first and second kind, respectively.

$p = (\text{length/diameter})$

$N_{zz} = 0.188$ and $N_{xx} = 0.406$

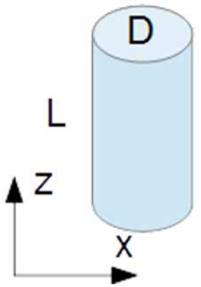

$D = 52\,nm$
$L = 100\,nm$
$V = 2.12 \cdot 10^{-22}\,m^3$

La anisotropía magnética está dominada por la energía magnetoestática

$$K_{ME} = \frac{1}{2}\mu_0(N_x - N_Z){M_S}^2 = 4.21 \cdot 10^4\, J/m^3 \;\gg K_{Nickel} \approx 5 \cdot 10^2\, J/m^3$$

PHYSICAL REVIEW B, VOLUME 65, 144417

Micromagnetic behavior of electrodeposited cylinder arrays

C. A. Ross,[1,*] M. Hwang,[1] M. Shima,[1] J. Y. Cheng,[1] M. Farhoud,[2] T. A. Savas,[3] Henry I. Smith,[2] W. Schwarzacher,[4] F. M. Ross,[5] M. Redjdal,[6] and F. B. Humphrey[6]

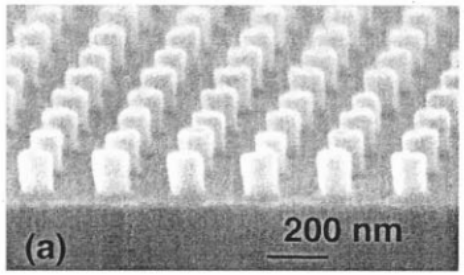
(a)
200 nm

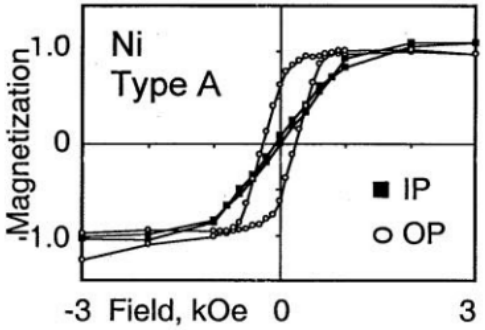
Ni
Type A
Magnetization
1.0
0
-1.0
IP
OP
-3 Field, kOe 0 3

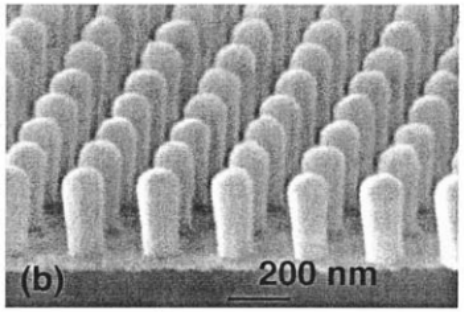
(b)
200 nm

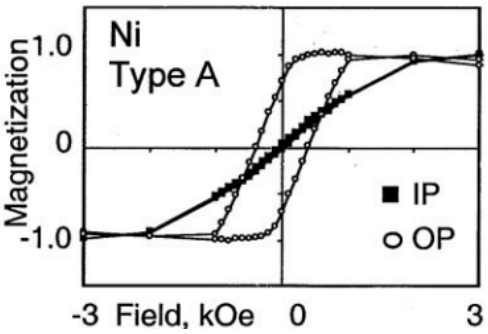
Ni
Type A
Magnetization
1.0
0
-1.0
IP
OP
-3 Field, kOe 0 3

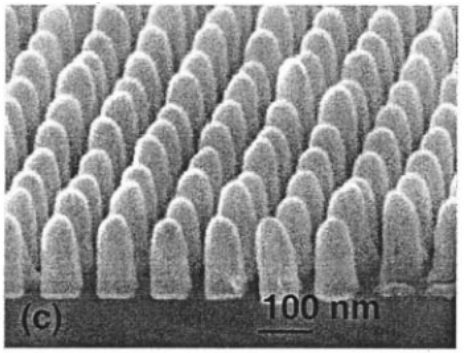
(c)
100 nm

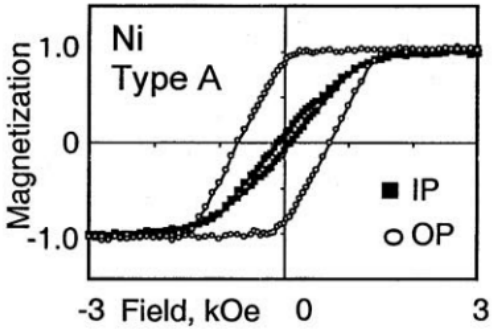
Ni
Type A
Magnetization
1.0
0
-1.0
IP
OP
-3 Field, kOe 0 3

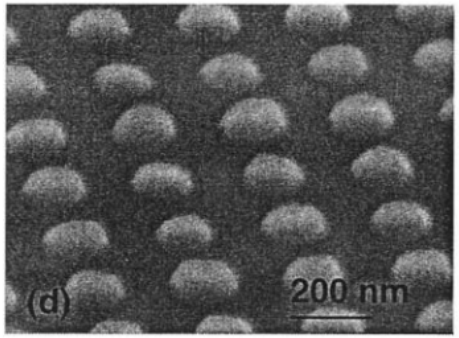
(d)
200 nm

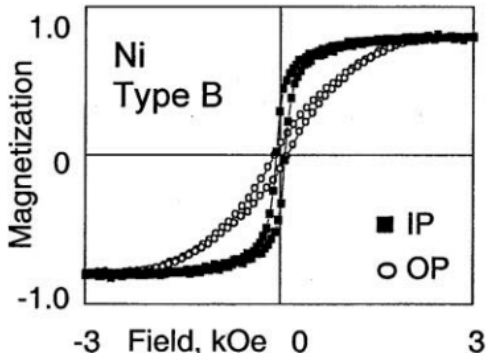
Ni
Type B
Magnetization
1.0
0
-1.0
IP
OP
-3 Field, kOe 0 3

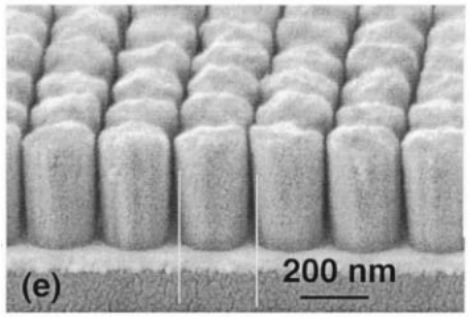
(e)
200 nm

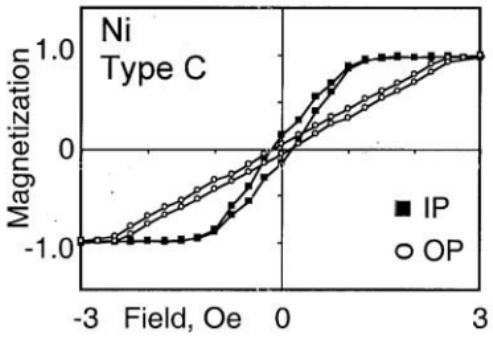
Ni
Type C
Magnetization
1.0
0
-1.0
IP
OP
-3 Field, Oe 0 3

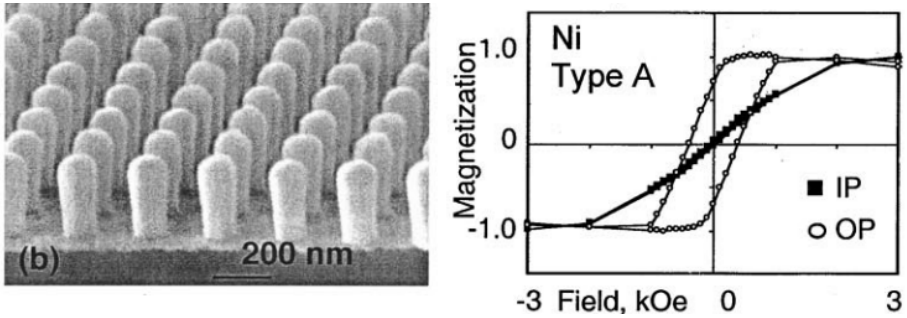

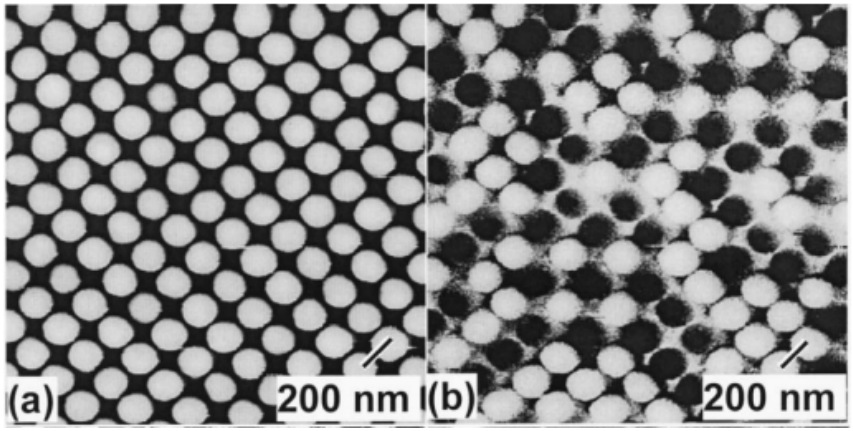

FIG. 3. (a) Topographic, and (b) magnetic image of an area of the Ni sample of Fig. 1(b) in its as-deposited condition.

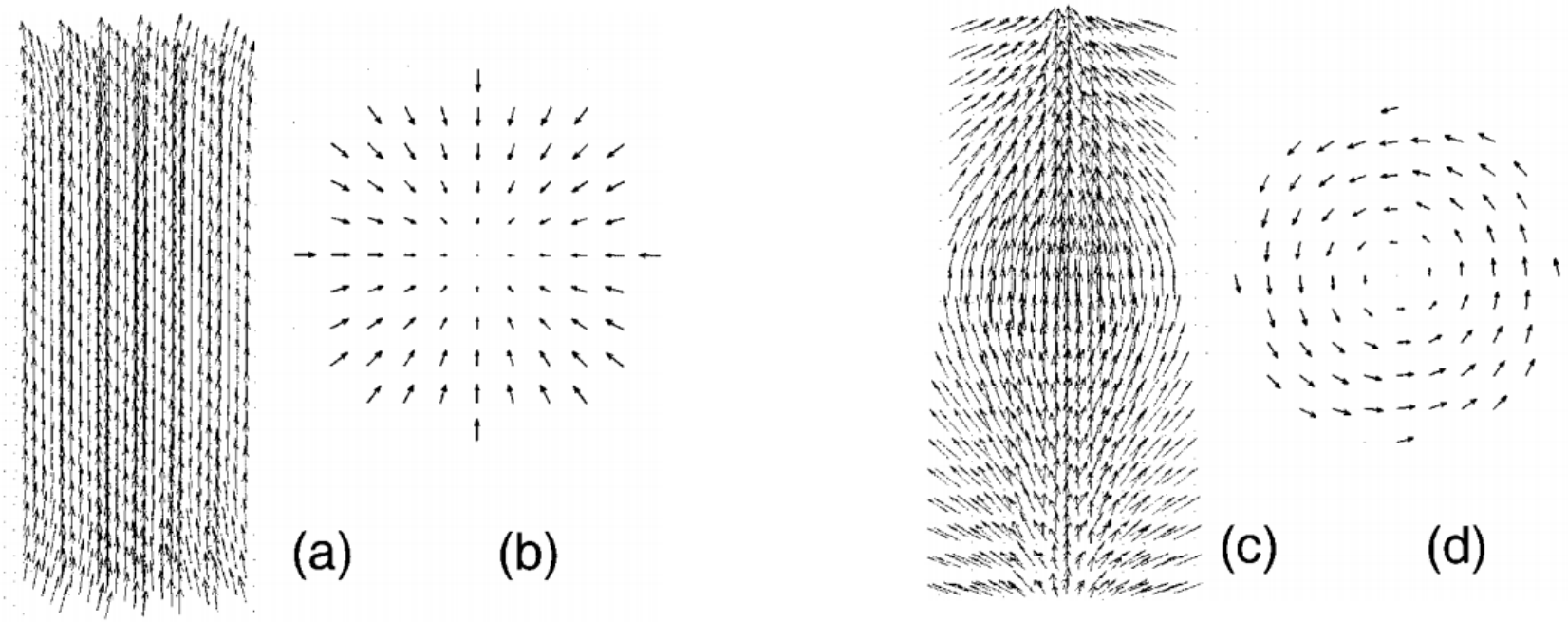

FIG. 4. Calculated remanent magnetization distributions in cylindrical particles. (a) Side view and (b) bottom face of a cylinder of aspect ratio $R=2.1$ and diameter $d=2.61\lambda_{ex}$, showing a flower state. (c) Side view and (d) top face of cylinder with $R=2.1$, and $d=6.1\lambda_{ex}$, showing a vortex state. The arrow lengths in (b) and (d) are plotted at different scales for clarity.

magnetic exchange length

$$\xi_e = \sqrt{\frac{4\pi A}{\mu_0 M_s^2}}$$ ← exchange stiffness

R (=height/diameter)

(i) the magnetic exchange length $\xi_e = \sqrt{\frac{4\pi A}{\mu_0 M_s^2}}$

(ii) on the aspect ratio λ

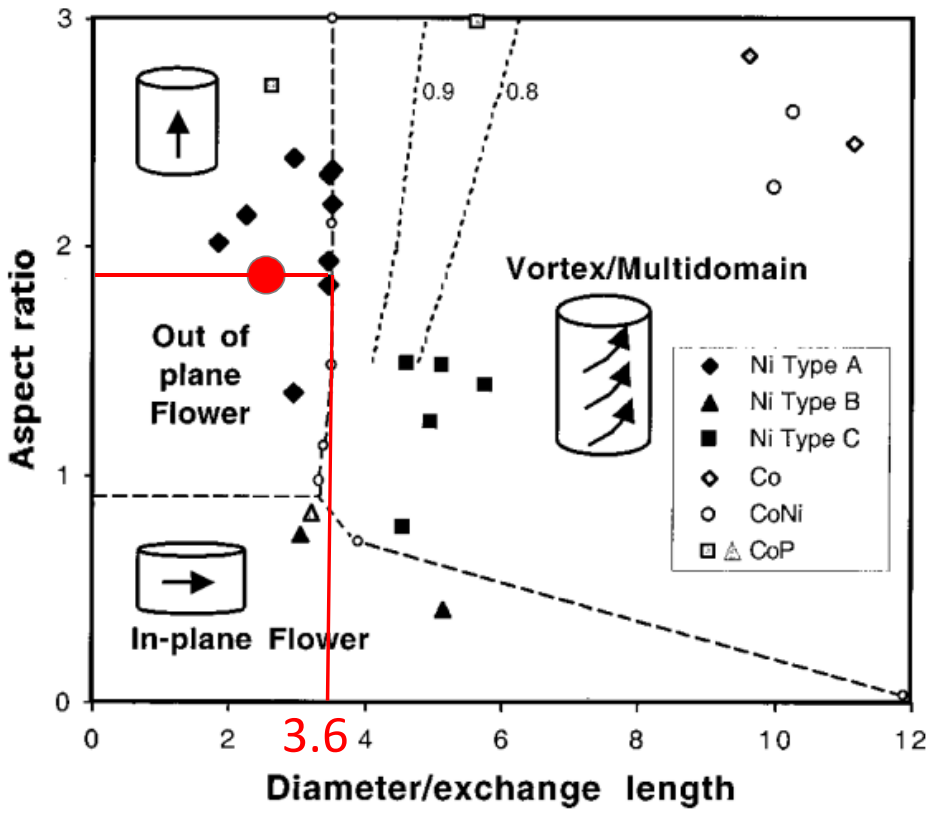

For nickel, $A = 1 \times 10^{-11}$ J/m

$\xi_e = 21$ nm

Diámetro D = 52 ± 2 nm = 2.55 ξe
Longitud L = 100 ± 6 nm
Relación de aspecto λ=1.9±0,1

For aspect ratio R = 1.92:

$D_{CR} \approx 3.6\xi_e$

D_{CR} = 75nm

they are single domain

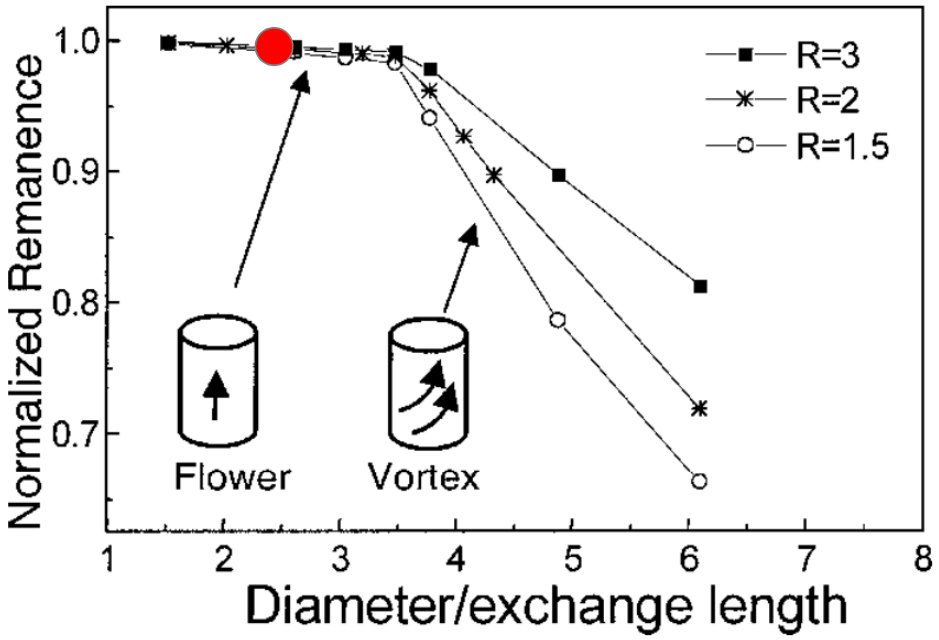

FIG. 5. Calculated remanence along the cylinder axis as a function of cylinder diameter, for three different aspect ratios R. The flower state has a remanence close to 1, which decreases as the vortex develops.

IV. EFFECTIVE DEMAGNETIZING TENSOR MODEL

magnetic susceptibility $\boldsymbol{\chi}$ second rank tensor
anisotropy of the magnetic material

component χ_{ij} of the differential susceptibility tensor $\boldsymbol{\chi}$ describes the magnetization variation in the ith direction from an incremental change in the jth direction of the applied field. Its 3×3 matrix components are defined as $\chi_{ij} = \frac{\partial M_i}{\partial H_j}$.

appropriate choice of coordinate system

three independent components in a diagonal form

privileged directions of the magnetization parallel to the chosen coordinate system

x is parallel to the plane of the alumina membrane

z parallel to the NP main axis

cylindrical geometry

two independent components

reducing the susceptibility to a 2×2 matrix:

$$\chi = \begin{bmatrix} \chi_{xx} & 0 \\ 0 & \chi_{zz} \end{bmatrix}$$

magnetostatic interactions between NPs

$$\vec{H}^E = \vec{H}^A + \vec{H}^D$$

$$\vec{H}^D = -\boldsymbol{N}^E \vec{M}$$

effective demagnetizing tensor

extrinsic effects

measured susceptibility

spatial distribution

apparent susceptibility tensor κ

$$\kappa_{ij} = \frac{\partial M_i}{\partial H_j^A}\Big|_{M_i=0}$$

---

true susceptibility tensor χ

$$\chi_{ij} = \frac{\partial M_i}{\partial H_j^E}\Big|_{M_i=0}$$

intrinsic one

NPs would have if they were noninteracting

$$\vec{M} = \boldsymbol{\kappa}\vec{H}^A = \boldsymbol{\chi}\vec{H}^E \qquad\qquad \vec{H}^E = \vec{H}^A - \boldsymbol{N}^E\vec{M}$$

The relation between them is given by:

$$\boldsymbol{\kappa} = (\boldsymbol{\chi}\boldsymbol{N}^E + \boldsymbol{I})^{-1}\boldsymbol{\chi}$$

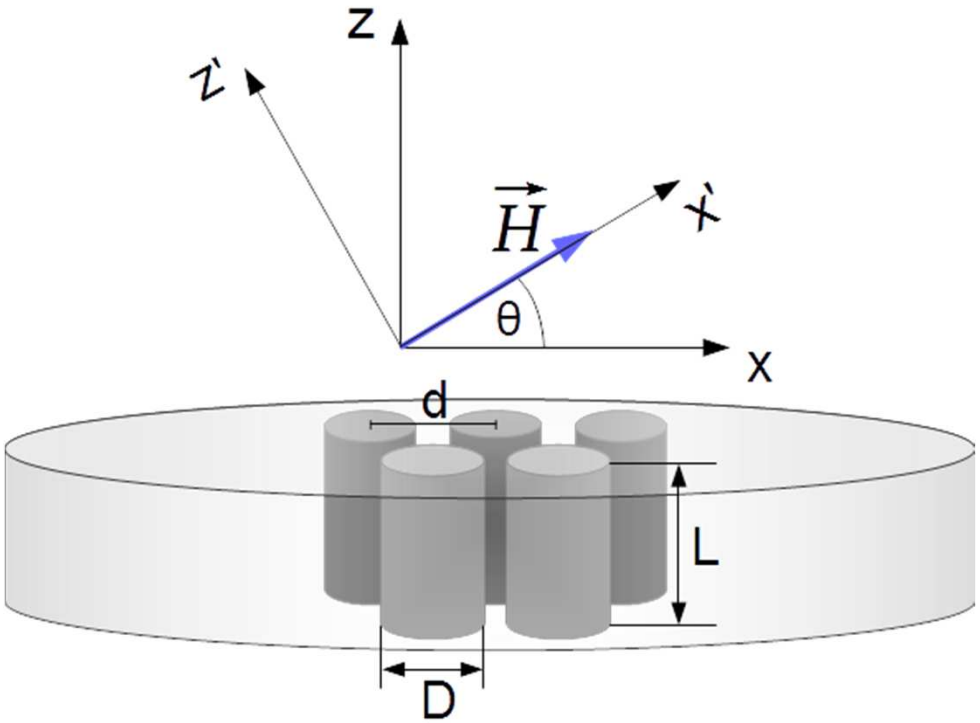

(x', z') where

$$\begin{bmatrix} x' \\ z' \end{bmatrix} = \boldsymbol{R}(\theta) \begin{bmatrix} x \\ z \end{bmatrix}$$

being

$$\boldsymbol{R}(\theta) = \begin{bmatrix} \cos\theta & -\sin\theta \\ \sin\theta & \cos\theta \end{bmatrix}$$

the rotation matrix

(counterclockwise through an angle θ)

$$\boldsymbol{\kappa}' = \boldsymbol{R}^{-1}(\theta)\boldsymbol{\kappa}\boldsymbol{R}(\theta)$$

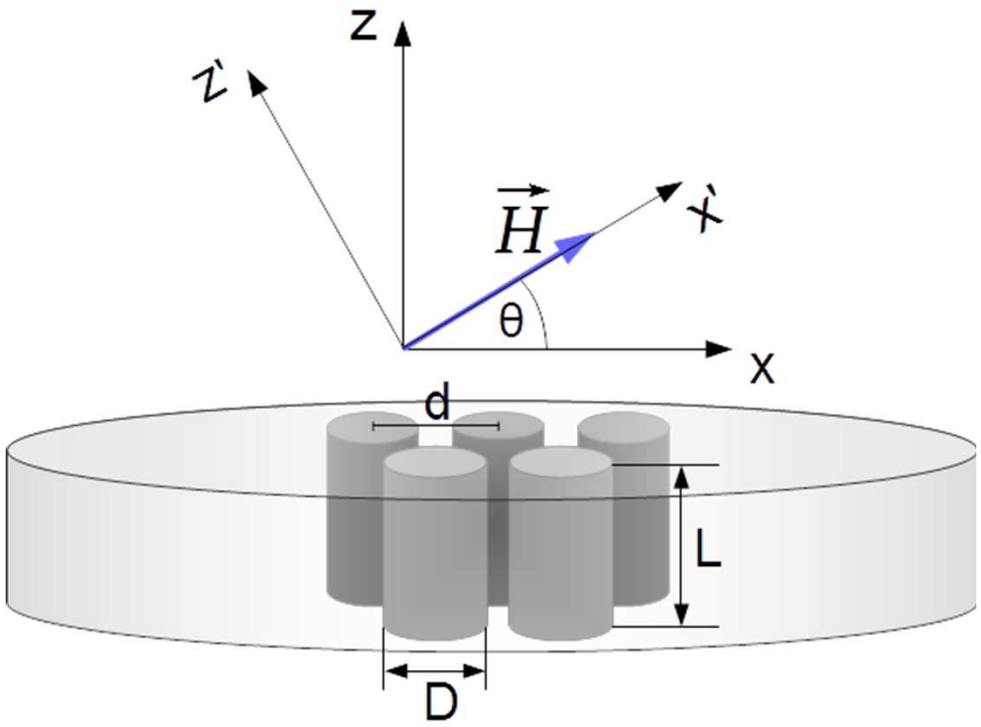

$$M'_x = \kappa'_{xx} H'^A_x + \kappa'_{zz} H'^A_z$$

as in the prime basis $H'^A_z = 0$

$$\text{thus } \kappa'_{xx} = \frac{\partial M'_x}{\partial H'^A_x}\Big|_{M'_x=0}$$

directly measure the κ'_{xx}

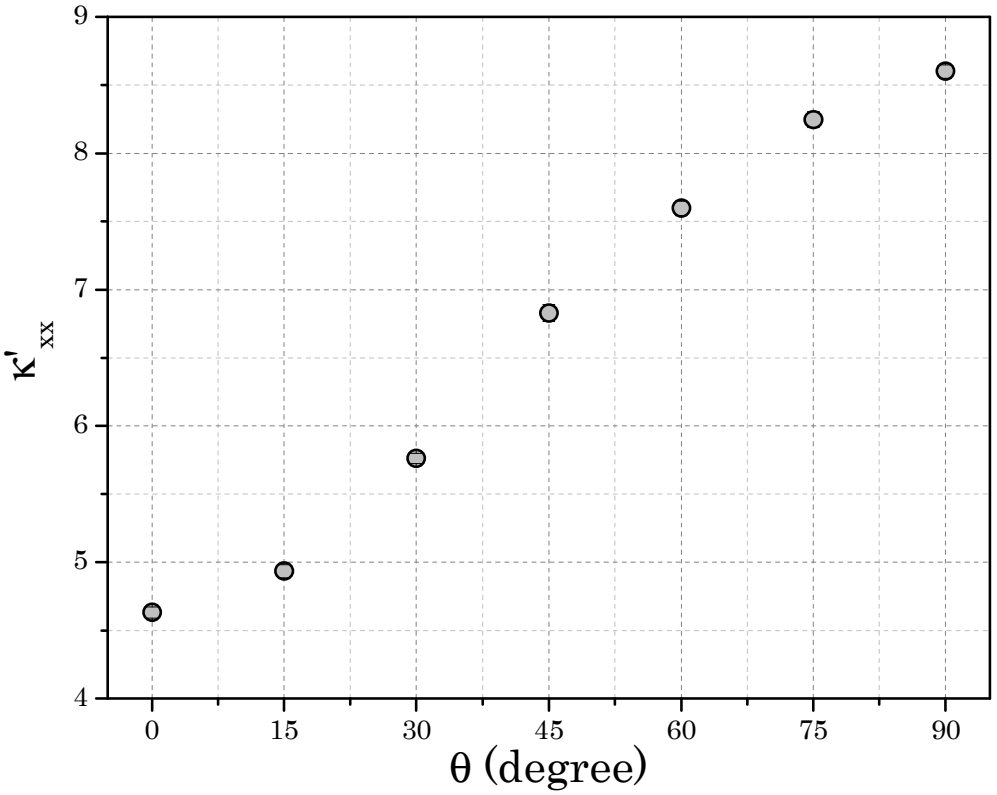

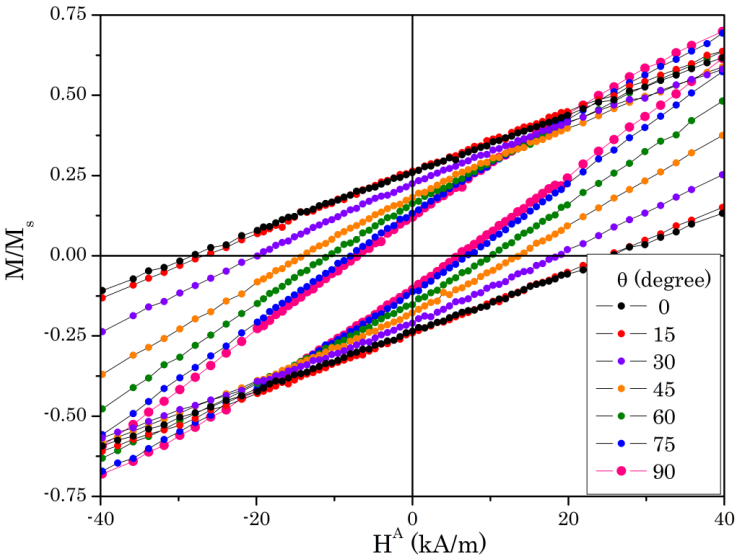

directly measure the κ'_{xx}

FIG. 4. Circles: Initial slope $\kappa'_{xx} = \frac{\partial M'_x}{\partial H'^A_x}|_{M'_x=0}$ extracted experimentally at different angles of the applied field.

values of κ'_{xx} obtained at

- $\theta = 0^\circ \longrightarrow \kappa_{xx} = 4.63 \pm 0.04$
- $\theta = 90^\circ \longrightarrow \kappa_{zz} = 8.60 \pm 0.05$

easy magnetization
axis is normal to the sample plane

parallel to the NP axes

simple isolated pillar without magnetostatic interactions

La anisotropía magnética está dominada por la energía magnetoestática

$$K_{ME} = \frac{1}{2}\mu_0 (N_x - N_Z) {M_S}^2 = 4.21 \cdot 10^4\, J/m^3$$

$$\sigma = \frac{V K_{\mathrm{ME}}}{k_B T} = 2.2 \times 10^3$$

As $\sigma \gg 1 \longrightarrow$ Stoner-Wohlfarth

$$\chi_{xx} \approx \frac{\mu_0 M_s^2}{2K_{\mathrm{ME}}} \approx 4.6$$

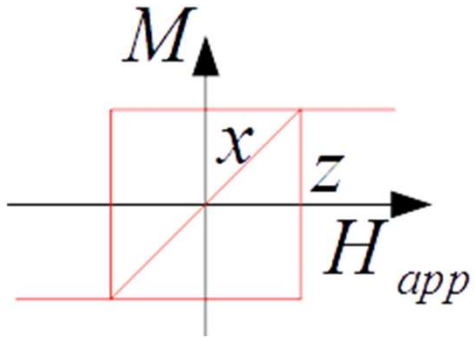

$$\chi_{zz} \to \infty$$

apparent susceptibility

$$\kappa_{xx} = 4.63 \pm 0.04$$

$$\kappa_{zz} = 8.60 \pm 0.05$$

Stoner-Wohlfarth

$$\chi_{xx} \approx \frac{\mu_0 M_s^2}{2K_{\mathrm{ME}}} \approx 4.6$$

$$\chi_{zz} \to \infty$$

$$\chi_{xx} \approx \kappa_{xx} \text{ but } \chi_{zz} \gg \kappa_{zz}$$

dipolar interaction effects are anisotropic

$$N_{uu}^{E} = \frac{\varphi}{\gamma^3}\left[N_{uu}^{c}\left(1 - \frac{\varphi_c}{\gamma_c^3}\right) + N_{uu}^{s}\frac{\varphi_c}{\gamma_c^3}\right]$$

$$\gamma = \frac{d}{D} \qquad \gamma_c = \frac{d_c}{D_c}$$

$$N_{uu}^{E} = \frac{\varphi}{\gamma^3}N_{uu}^{c} + \frac{\varphi_c}{\gamma_c^3}\frac{\varphi_c}{\gamma_c^3}\left(N_{uu}^{s} - N_{uu}^{c}\right)$$

Fracción de volumen de NP en cluster

Fracción de volumen de NP en muestra

φ_c and γ_c are equal to unity

$$N_{uu}^{E} = \frac{\varphi}{\gamma^3} N_{uu}^{s}$$

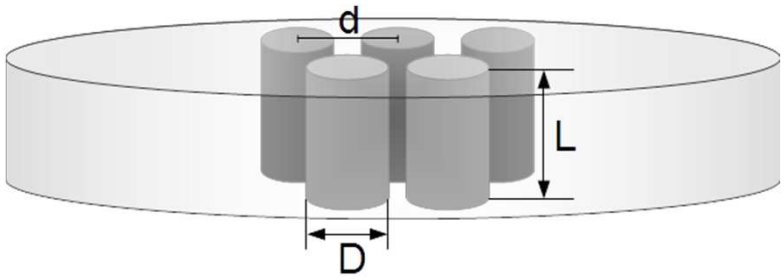

$$\gamma = \frac{d}{D}$$

$$\varphi = \frac{\pi}{4\cos\frac{\pi}{6}} \approx 0.907$$

Estimation of φ

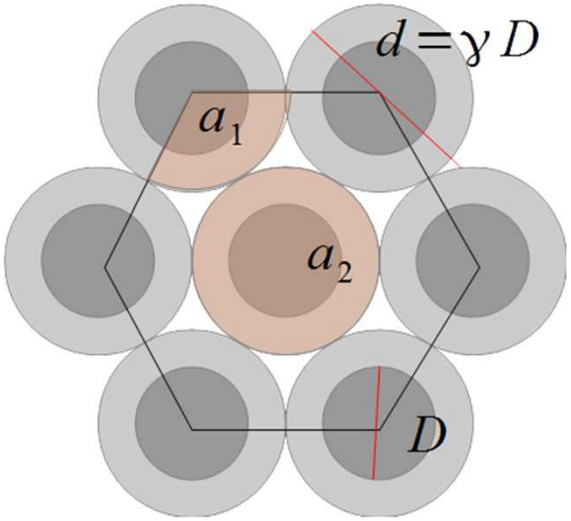

$$a_1 = \theta \left(\frac{d}{2}\right)^2 = \frac{\pi d^2}{3 \cdot 4}$$

$$a_2 = \pi \left(\frac{d}{2}\right)^2 = \frac{\pi d^2}{4}$$

$$\phi = \frac{a_2 + 6 a_1}{6 a_3}$$

$$\phi = \frac{\pi}{4 \cos(\pi/6)} \approx 0{,}907$$

$$\frac{\varphi}{\gamma^3} = 0.096$$

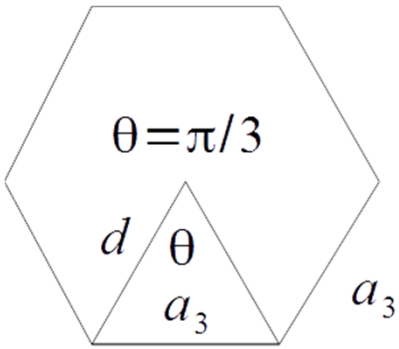

$$a_3 = \frac{d^2}{2} \cos(\pi/6)$$

$$D = 52\,nm$$

$$L = 100\,nm$$

$$d = 110\,nm$$

$$\gamma = 2.115$$

Considering the shape of the specimen

$$N_{uu}^{E} = \frac{\varphi}{\gamma^3} N_{uu}^{s}$$

$$N_{xx}^{s} \approx 0 \text{ and } N_{zz}^{s} \approx 1$$

$$N_{zz}^{E} = \frac{\varphi}{\gamma^3} \approx 0.096$$

$$N_{xx}^{E} \approx 0$$

Once $\boldsymbol{N}^E$ is known

$$\vec{H}^D = -\boldsymbol{N}^E \vec{M}$$

$$\vec{H}^E = \vec{H}^A + \vec{H}^D$$

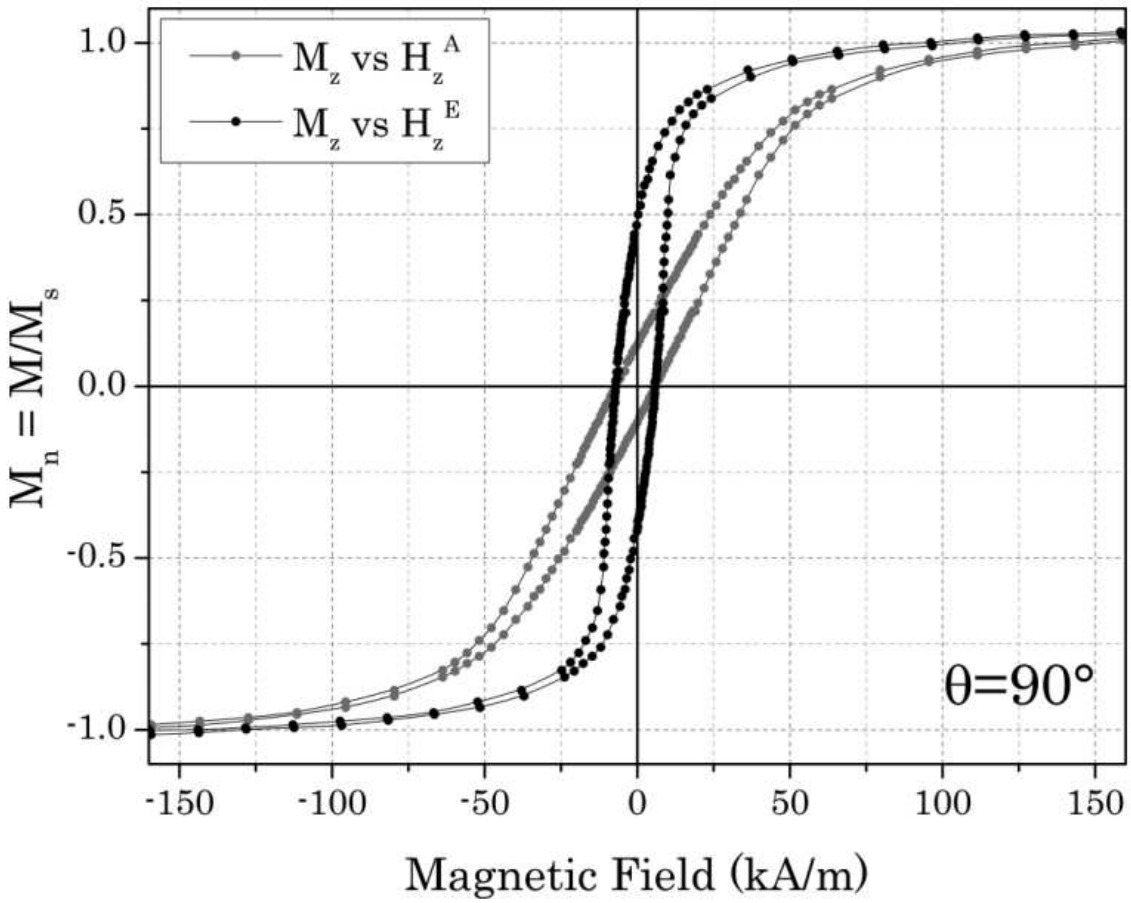

FIG. 5. Experimental dependence of M_z versus the applied (H_z^A) and effective (H_z^E) fields at $\theta = 90°$. H_z^E was calculated using $N_{zz}^E = 0.096$ from Eq. (4).

recovering of χ_{zz} from its apparent value κ_{zz}

in this case $\chi_{zz} > \kappa_{zz}$

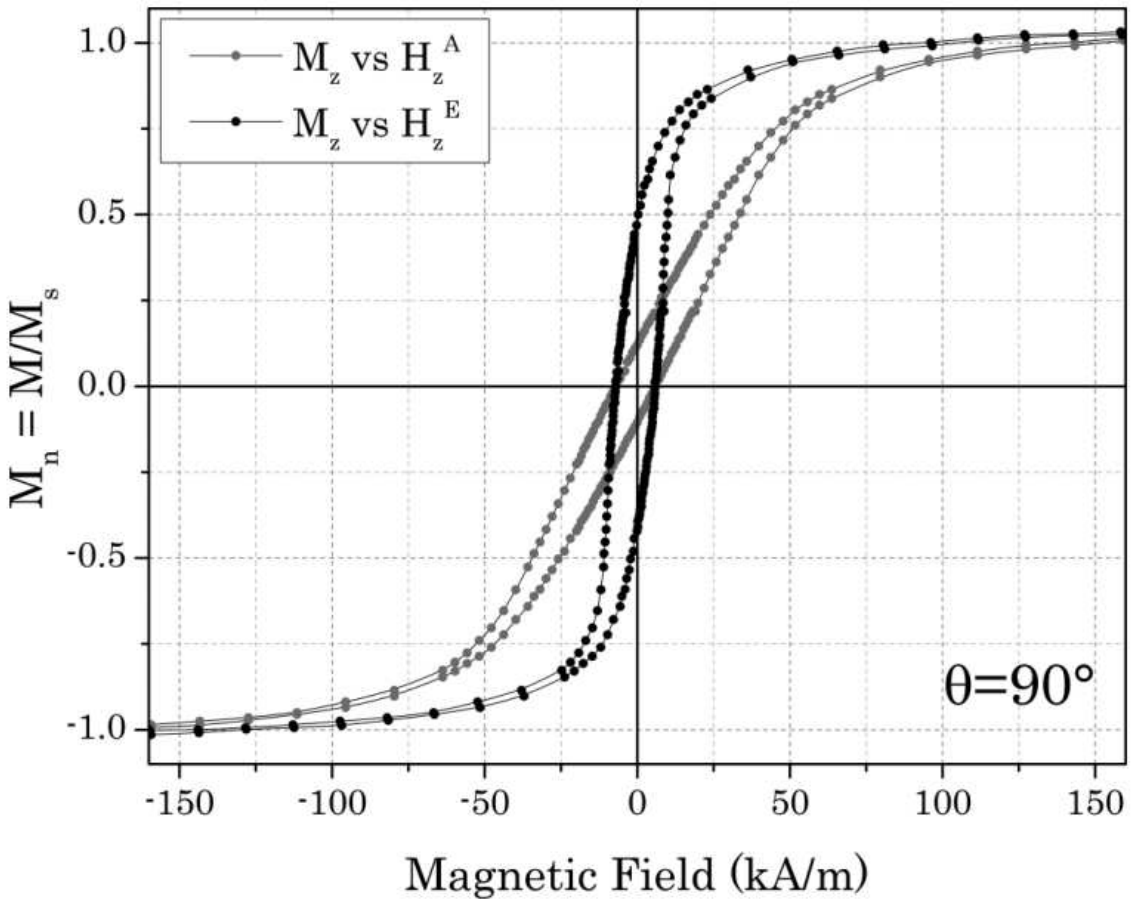

FIG. 5. Experimental dependence of M_z versus the applied (H_z^A) and effective (H_z^E) fields at $\theta = 90°$. H_z^E was calculated using $N_{zz}^E = 0.096$ from Eq. (4).

Once $\boldsymbol{N}^E$ is determined, it is possible to obtain an expression of $\boldsymbol{\kappa}'$ in terms of the components of $\boldsymbol{\chi}$:

$$\boldsymbol{\kappa}' = \boldsymbol{R}^{-1}(\theta)\boldsymbol{\kappa}\boldsymbol{R}(\theta) \qquad \boldsymbol{\kappa} = (\boldsymbol{\chi}\boldsymbol{N}^E + \boldsymbol{I})^{-1}\boldsymbol{\chi}$$

$$\boldsymbol{\kappa}' = \begin{bmatrix} \frac{\chi_{xx}}{1+N^E_{xx}\chi_{xx}}\cos^2\theta + \frac{\chi_{zz}}{1+N^E_{zz}\chi_{zz}}\sin^2\theta & \left(\frac{\chi_{zz}}{1+N^E_{zz}\chi_{zz}} - \frac{\chi_{xx}}{1+N^E_{xx}\chi_{xx}}\right)\cos\theta\sin\theta \\ \left(\frac{\chi_{zz}}{1+N^E_{zz}\chi_{zz}} - \frac{\chi_{xx}}{1+N^E_{xx}\chi_{xx}}\right)\cos\theta\sin\theta & \frac{\chi_{xx}}{1+N^E_{xx}\chi_{xx}}\cos^2\theta + \frac{\chi_{zz}}{1+N^E_{zz}\chi_{zz}}\sin^2\theta \end{bmatrix}$$

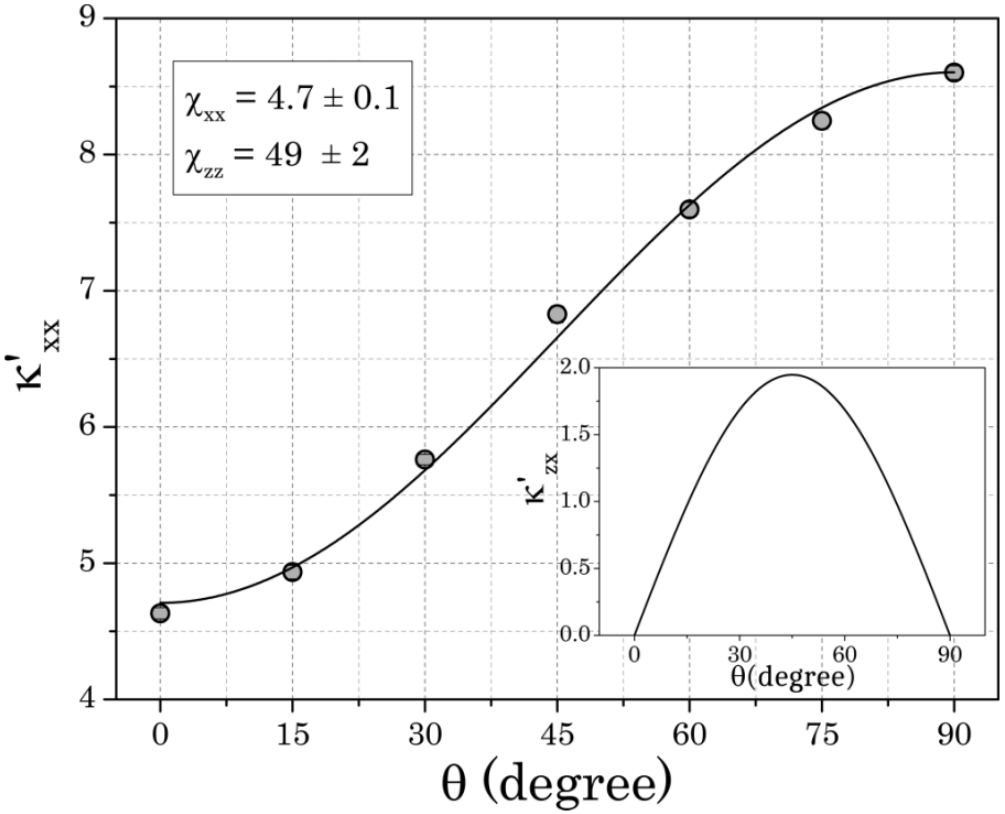

$$\kappa'_{xx} = \frac{\chi_{xx}}{1+N^E_{xx}\chi_{xx}}\cos^2\theta + \frac{\chi_{zz}}{1+N^E_{zz}\chi_{zz}}\sin^2\theta$$

$$\chi_{xx} = 4.7 \pm 0.1 \text{ and } \chi_{zz} = 49 \pm 2$$

Stoner-Wohlfarth

$$\chi_{zz} \gg \chi_{xx} \text{ and } \chi_{xx} \approx 4.6$$

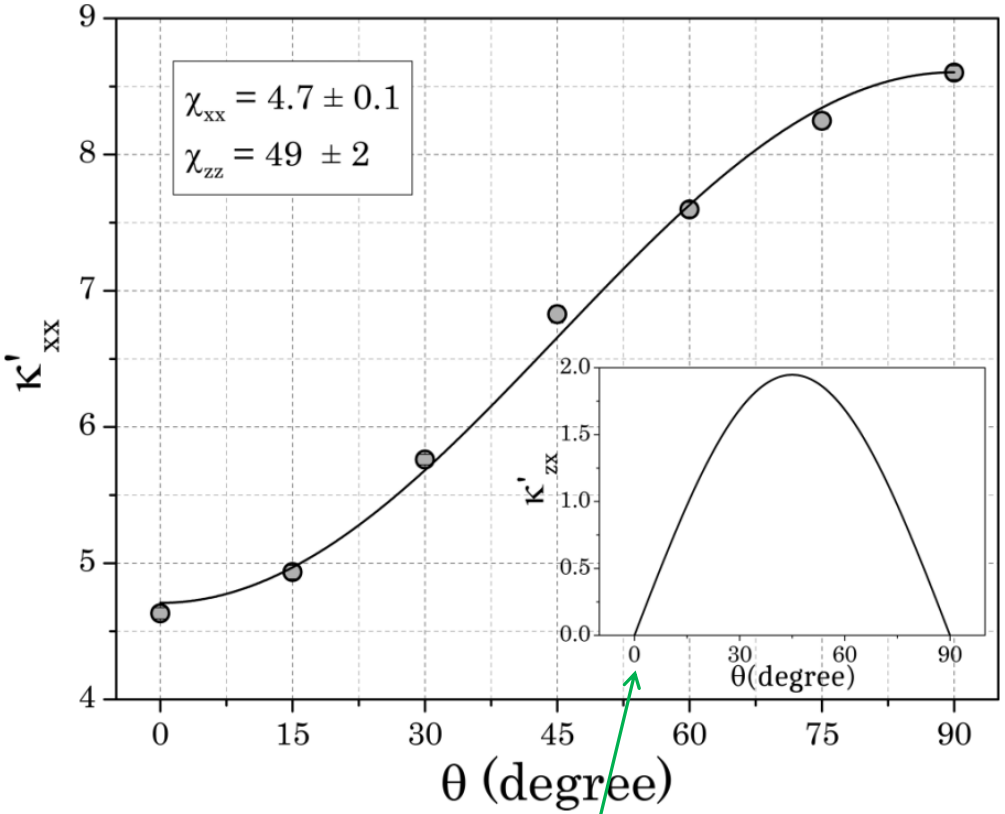

magnetization perpendicular to the applied magnetic field

when the field is applied along a nonprincipal direction, $\vec{M}$ has a component perpendicular to $\vec{H}^A$

$$\boldsymbol{\kappa}' = \begin{bmatrix} \frac{\chi_{xx}}{1+N^E_{xx}\chi_{xx}}\cos^2\theta + \frac{\chi_{zz}}{1+N^E_{zz}\chi_{zz}}\sin^2\theta & \left(\frac{\chi_{zz}}{1+N^E_{zz}\chi_{zz}} - \frac{\chi_{xx}}{1+N^E_{xx}\chi_{xx}}\right)\cos\theta\sin\theta \\ \left(\frac{\chi_{zz}}{1+N^E_{zz}\chi_{zz}} - \frac{\chi_{xx}}{1+N^E_{xx}\chi_{xx}}\right)\cos\theta\sin\theta & \frac{\chi_{xx}}{1+N^E_{xx}\chi_{xx}}\cos^2\theta + \frac{\chi_{zz}}{1+N^E_{zz}\chi_{zz}}\sin^2\theta \end{bmatrix}$$

$$\chi' = \begin{bmatrix} \chi_{xx}\cos^2\theta + \chi_{zz}\sin^2\theta & (\chi_{zz} - \chi_{zz})\cos\theta\sin\theta \\ (\chi_{zz} - \chi_{zz})\cos\theta\sin\theta & \chi_{zz}\cos^2\theta + \chi_{xx}\sin^2\theta \end{bmatrix}$$

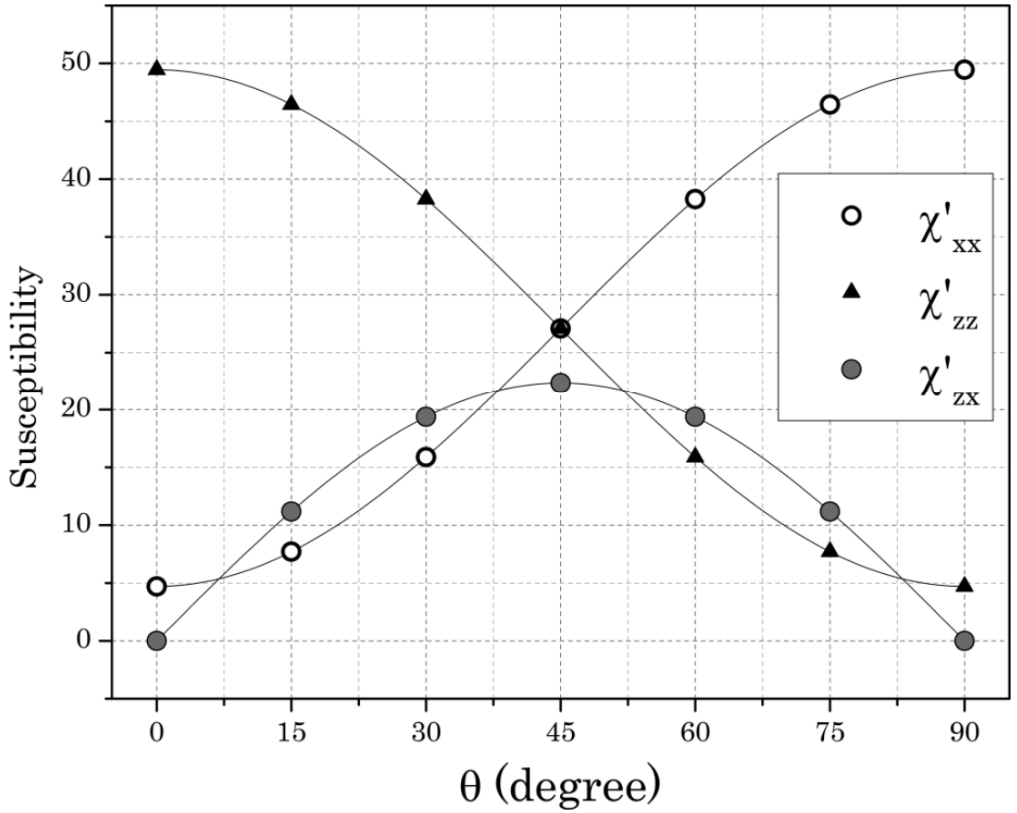

FIG. 6. χ'_{xx}, χ'_{zz}, and χ'_{xz} components as a function of the angle θ between magnetic field and x axis (parallel to the plane of the alumina membrane).

the angle α between the sample plane and the magnetization increment $\Delta\vec{M}$

$$\tan\alpha = \frac{1 + N_{xx}^{E}}{1 + N_{zz}^{E}} \left(\frac{\chi_{zz}}{\chi_{xx}} \right) \tan\theta$$

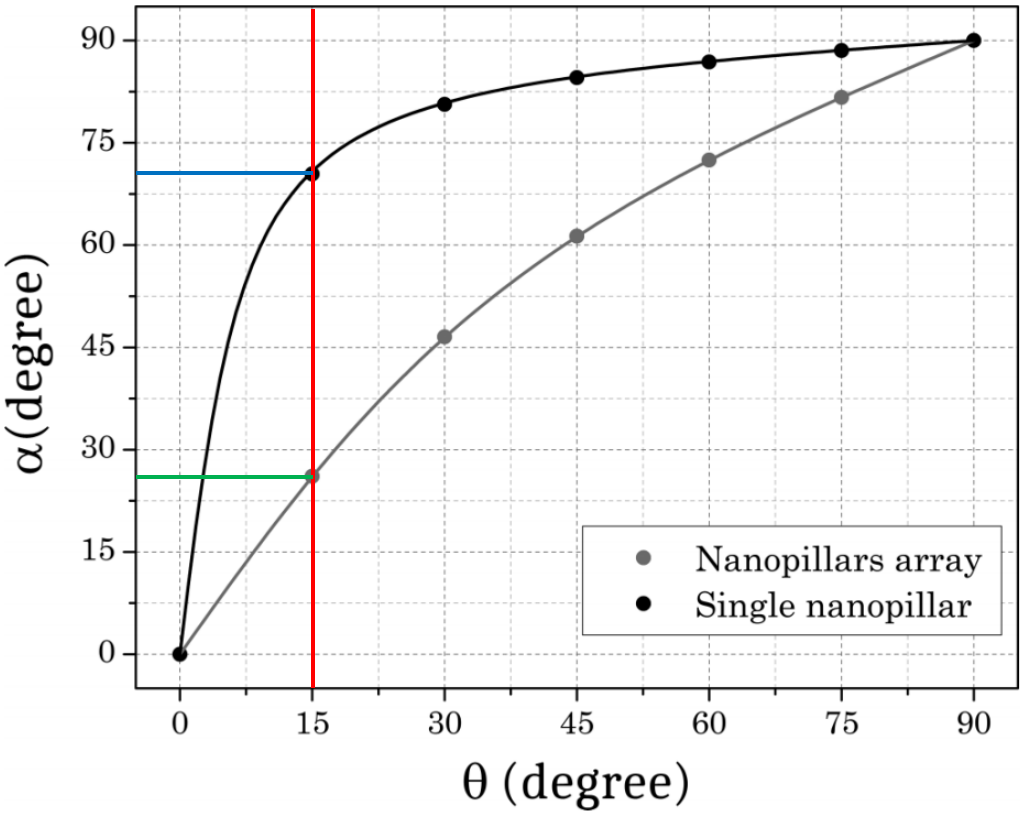

$$\tan\alpha = \frac{1 + N_{xx}^{E}}{1 + N_{zz}^{E}} \left(\frac{\chi_{zz}}{\chi_{xx}} \right) \tan\theta$$